Low-energy deuteron-induced reactions on ^{93}Nb

M. Avrigeanu,[1,*] V. Avrigeanu,[1] P. Bém,[2] U. Fischer,[3] M. Honusek,[2] A. J. Koning,[4] J. Mrázek,[2] E. Šimečková,[2,†] M. Štefánik,[2] and L. Závorka[2]

[1]*Horia Hulubei National Institute for Physics and Nuclear Engineering, P. O. Box MG-6, 077125 Bucharest-Magurele, Romania*
[2]*Euratom/IPP.CR Fusion Association, Nuclear Physics Institute, 25068 Řež, Czech Republic*
[3]*Euratom/FZK Fusion Association, Karlsruhe Institute of Technology (KIT), Hermann-von-Helmholtz-Platz, 1, 76344 Eggenstein-Leopoldshafen, Germany and*
[4]*Nuclear Research and Consultancy Group, P. O. Box 25, NL-1755 ZG Petten, The Netherlands*

(Received 17 May 2013; published 26 July 2013)

The activation cross sections of (d, p), $(d, 2n)$, $(d, 2np + nd + t)$, $(d, 2n\alpha)$, and $(d, p\alpha)$ reactions on ^{93}Nb were measured in the energy range from 1 to 20 MeV using the stacked-foil technique. Then, within a simultaneous analysis of elastic scattering and reaction data, the available elastic-scattering data analysis was carried out in order to obtain the optical potential for reaction cross-section calculations. Particular attention was paid to the description of the breakup mechanism and direct reaction stripping and pick-up, followed by pre-equilibrium and compound-nucleus calculations. The measured cross sections as well as all available deuteron activation data of ^{93}Nb were compared with results of local model calculations carried out using the codes FRESCO and STAPRE-H and both default and particular predictions of the code TALYS-1.4 and TENDL-2012-evaluated data.

DOI: 10.1103/PhysRevC.88.014612 PACS number(s): 24.10.Eq, 24.10.Ht, 25.45.De, 21.30.Fe

I. INTRODUCTION

The description of deuteron-nucleus interaction represents an important test for both reaction mechanism models and evaluation of nuclear data requested especially by research programs such as ITER [1], IFMIF [2], and SPIRAL2-NFS [3]. The weak binding energy of the deuteron, $B_d = 2.224$ MeV, is responsible for the high complexity of the interaction process that also involves a variety of reactions initiated by the neutron and proton following the deuteron breakup (BU). The difficulties in interpreting the deuteron-induced reaction data in terms of the usual reaction mechanism models have recently been reinvestigated [4–10], looking for a consistent way to include the breakup contribution within the activation cross-section calculations.

On the other hand, contributions of the (d, p) and (d, n) stripping as well as the (d, t) pick-up direct reactions (DR) have also been usually neglected or very poorly taken into account, in spite of their importance at low incident energies. Finally, the pre-equilibrium emission (PE) and evaporation from fully equilibrated compound nucleus (CN) become important when the incident energy is increased above the Coulomb barrier. However, even the PE and CN analysis has to take into account the decrease of the deuteron total reaction cross section due to the above-mentioned BU, stripping, and pick-up processes. The present work concerns a deeper understanding of the deuteron breakup, stripping, and pick-up reactions, and the better-known statistical emission, all together and consistently, for deuteron interaction with the ^{93}Nb target nucleus.

Since it is used as either pure metal or a component of various alloys due to the advantageous physical and chemical properties, the ^{93}Nb nucleus is quite important for nuclear technology. The monoisotopic nature makes easier the measurements of both neutron and charged-particle induced reactions on this target nucleus while the related nuclear model analysis may avoid difficulties met for elements with more stable isotopes. Unfortunately, the deuteron-induced activation on ^{93}Nb led mainly to isomeric states, while the model analysis of the isomeric cross sections for incident energies up to the upper limit of the low-energy range (50 MeV) presumes the account of the angular-momentum and parity conservation at any stage of the concerned nuclear interactions. Moreover, their accurate calculation needs a suitable description of two basic nuclear quantities, namely the nuclear level-density spin distribution and the radiative strength functions, both of them the object of intricate investigations. Altogether, there are only a few measurements performed for deuteron activation of ^{93}Nb [11,12] while their analysis is rather limited to global predictions and use of approximations.

The experimental setup and the measured data are described in Sec. II. Next, a consistent energy-dependent optical potential for deuterons on ^{93}Nb is discussed in Sec. III. Deuteron breakup effects on the ^{93}Nb activation data are established in Sec. IV. The one-nucleon transfer DR analysis using the computer code FRESCO [13] is described in Sec. V, followed by a discussion in Sec. VI of the local input parameter set involved in analysis of PE and CN processes using the code STAPRE-H [14]. The measured and calculated deuteron activation cross sections of ^{93}Nb are discussed in Sec. VII, including default and particular calculations performed using the code TALYS-1.4 [15] and evaluated data from the TENDL-2012 library [16]. Partial and preliminary results were presented elsewhere [8,9,17,18].

II. MEASUREMENTS

The irradiation was carried out using an external deuteron beam of the NPI variable-energy cyclotron U-120M

*marilena.avrigeanu@nipne.ro
†simeckova@ujf.cas.cz

operating in the negative-ion mode of acceleration. From the stripping-foil extractor the beam was delivered to the reaction chamber through beam line consisting of one dipole and two quadrupole magnets. The energy was determined with a resulting accuracy of 1.0%, and the full width at half-maximum (FWHM) spread of the incident beam up to 1.8% was observed.

The activation cross sections were measured by use of a stacked-foil technique. A collimated deuteron beam strikes the stack of foils in a Faraday-cup-like reaction chamber, enabling the cooling of stacked foils without a loss of accuracy in the beam current and charge monitoring (10%).

The high-purity Nb foils (Goodfellow product, 99.9% purity, 25 μm declared thickness) and Al (50 μm declared thickness) were weighed (within 2% of accuracy) to avoid relatively large uncertainties in the foil thickness declared by producer. The mean energy, energy thickness, and energy spread in each foil were set out by SRIM 2003 code [19]. The foils of examined element Nb were inserted in the chamber by turn with Al foils that were used for additional monitoring of the beam current and appropriate reduction of the deuteron energy as well.

Three irradiation runs were carried out to check internal consistency of the measurement. In addition, two measurements were performed at the lower energy of 13.86 MeV to obtain the ^{93}Nb(d, p)^{94}Nb^m reaction cross sections around the excitation function maximum. The characteristics of single runs are given in Table I.

The γ rays from the irradiated foils were measured repeatedly by a calibrated HPGe detector of 50% efficiency and of FWHM 1.8 keV at 1.3 MeV. Experimental reaction rates were calculated from the specific activities at the end of the irradiation and corrected to the decay during irradiation using total charge and foil characteristics as well. The measurement with different cooling times lasted up to 100 days after irradiation. The characteristics of the isotopes observed from irradiated Nb foils [20] are given in Table II.

The experimental cross-section data for the ^{93}Nb(d, $2n$)^{93}Mo^m, ^{93}Nb(d, x)^{92}Nb^m, ^{93}Nb(d, $p\alpha$)^{90}Y^m, ^{93}Nb(d, $2n\alpha$)^{89}Zr, and ^{93}Nb(d, p)^{94}Nb^m reactions are shown in Table III. They are in excellent agreement with previous works [11,12]. The cross-section values for the ^{93}Nb(d, p)^{94}Nb^m strongly depend on the intensity of the single γ 871.1-keV line (Table II).

TABLE I. Characteristics of single runs.

Run No	Initial energy (MeV)	Total charge (μC)	Irradiation time (s)	Mean current (μA)
1	19.64	513.6	2610	0.197
2	19.60	245.8	1182	0.208
3	19.60	271.7	1238	0.219
4	13.86	160.6	602	0.267
5	13.86	162.6	604	0.269

TABLE II. Half-lives, main γ lines, and their intensities of the isotopes observed from irradiated Nb foils [20].

Isotope	$T_{1/2}$	E_γ(keV)	I_γ(%)
^{93}Mo^m	6.85 h	684.7	99.7
		1477.1	99.1
		263.1	56.7
^{92}Nb^m	10.15 d	934.5	99
		912.7	1.78
^{90}Y^m	3.19 h	202.5	97.5
		479.2	90.7
^{89}Zr	78.41 h	908.9	100
^{94}Nb^m	6.263 min	871.1	0.50

III. ENERGY-DEPENDENT OPTICAL POTENTIAL

The deuteron total reaction cross sections are less accurately described since, unlike the nucleon case, there are no global optical model potentials (OMP) which describe sufficiently well the scattering data over wide ranges of energy and target nuclei. However, a prime interest for the OMP parameters is motivated by their further use within analysis of all deuteron interaction cross sections. Unfortunately, the few angular-distribution measurements of elastic-scattered deuterons on ^{93}Nb [21,22] do not allow an extended OMP analysis.

Actually, previous OMP analyses on ^{6,7}Li [23,24], ^{27}Al [4,5], $^{54,56,58,\text{nat}}$Fe [25], ^{59}Co, and ^{93}Nb [8,18] showed that no global OMP describes sufficiently well the elastic-scattering data for deuterons in the energy range up to 20 MeV. Therefore, we have fitted the available experimental elastic-scattering angular distributions for ^{93}Nb (Fig. 1) by adjusting several parameters (Table IV) of the Daehnick *et al.* [26] OMP. A good description of the data has been obtained as it results from comparison with the calculated values using the presently adjusted OMP parameters and previous potentials [26–28] within the widely used TALYS code [15]. Also shown in Fig. 1(b) are the total reaction cross sections σ_R for deuterons incident on ^{93}Nb calculated by using the same potentials. A similar comparison with the results obtained by using another previous potential [29] and the TALYS default option based on the Watanabe folding approach [30] was formerly given [25]. Unfortunately, there are no available measured total reaction cross sections. One may note the differences up to 20% between the various predictions while the OMP parameters of the present work, obtained by fit of the elastic-scattering angular distributions shown in Fig. 1(a), led to intermediary values.

IV. DEUTERON BREAKUP EFFECTS ON ACTIVATION CROSS SECTIONS

A. BU components

The physical picture of the deuteron breakup, in the Coulomb and nuclear fields of the target nucleus, considers two distinct chains. These are the elastic-breakup (EB), in which the target nucleus remains in its ground state and none of the deuteron nucleons interacts with it, and the inelastic-breakup or breakup fusion (BF), where one of the deuteron nucleons

TABLE III. Measured reaction cross sections (mb) for deuterons incident on the ^{93}Nb nucleus. The energy errors take into account the energy thickness of each foil and the initial-energy spread error. Cross-section errors are composed of statistical errors in activity determination and systematical errors of charge measurement uncertainty (10%), foil thickness uncertainty (2%), and uncertainty of HPGe detector efficiency determination (2%). The uncertainties are given in parentheses, in units of the last digit.

Energy	Reaction				
(MeV)	^{93}Nb$(d, 2n)^{93}$Mo^m	^{93}Nb$(d, x)^{92}$Nb^m	^{93}Nb$(d, p\alpha)^{90}$Y^m	^{93}Nb$(d, 2n\alpha)^{89}$Zr	^{93}Nb$(d, p)^{94}$Nb^m
19.35 (60)	101.7 (106)	30.1 (32)	0.257 (28)	1.474 (159)	35.2 (155)
18.89 (60)	108.2 (114)	26.9 (28)	0.235 (26)	0.956 (110)	
18.79 (63)	108.1 (113)	17.7 (19)	0.158 (19)	0.451 (58)	51.9 (74)
17.87 (64)	124.1 (130)	21.5 (23)		0.214 (25)	42.2 (116)
17.72 (63)	113.8 (119)	13.9 (15)	0.120 (18)	0.086 (9)	
17.38 (64)	120.4 (127)	15.0 (16)		0.124 (15)	56.6 (86)
16.53 (64)	115.5 (121)	9.37 (99)	0.079 (36)		
16.25 (65)	126.2 (134)	10.2 (11)	0.057 (18)		61.8 (110)
15.77 (63)	118.1 (126)	9.20 (96)	0.056 (17)		63.7 (70)
15.38 (66)	108.8 (113)	7.24 (76)	0.041 (21)		
14.53 (67)	111.2 (117)	6.73 (71)			74.4 (82)
14.05 (68)	93.2 (97)	5.91 (63)			
14.03 (69)	103.0 (109)	6.63 (70)			78.2 (88)
13.52 (59)					85.6 (215)
12.89 (61)					104 (18)
12.73 (71)	73.8 (77)	4.89 (51)			
12.64 (71)	80.4 (84)	5.47 (57)			90.2 (111)
12.18 (61)					108 (13)
12.09 (71)	75.7 (81)	5.01 (53)			
11.51 (62)					101 (12)
11.31 (72)	54.3 (57)	3.35 (41)			
10.52 (75)	53.2 (56)	3.91 (41)			108 (12)
10.01 (66)					116 (13)
9.92 (75)	44.4 (47)	3.40 (46)			
9.77 (76)	31.0 (33)	2.63 (28)			
9.10 (69)					127 (8)
8.37 (68)					136 (14)
8.05 (79)	9.6 (10)	1.00 (11)			
8.04 (83)	19.5 (21)	1.80 (20)			128 (14)
7.37 (83)	11.9 (12)	1.30 (14)			
7.24 (78)					128 (8)
6.48 (75)					111 (13)
6.06 (88)	0.264 (28)	0.157 (25)			
4.94 (92)					58.5 (36)
4.13 (91)					25.3 (28)
3.43 (111)	0.0049 (5)	0.131 (24)			
1.28 (161)					0.64 (13)

interacts with the target nucleus while the remaining one is detected.

An empirical parametrization of the total proton-emission breakup fraction $f_{\mathrm{BU}}^{(p)} = \sigma_{\mathrm{BU}}^{p}/\sigma_R$ and the elastic breakup fraction $f_{\mathrm{EB}} = \sigma_{\mathrm{EB}}/\sigma_R$ were obtained [4] through analysis of the experimental systematics [31,32] of proton-emission spectra and angular distributions of deuteron-induced reactions on target nuclei from Al to Pb, at incident energies from 15 to 80 MeV. The dependence of these fractions on the deuteron incident energy E and the charge Z and atomic number A of the target nucleus is [4,10]

$$f_{\mathrm{BU}}^{(n/p)} = 0.087 - 0.0066Z + 0.00163ZA^{1/3} + 0.0017A^{1/3}E - 0.000002ZE^2, \quad (1)$$

$$f_{\mathrm{EB}} = 0.031 - 0.0028Z + 0.00051ZA^{1/3} + 0.0005A^{1/3}E - 0.000001ZE^2. \quad (2)$$

Consequently, the inelastic-breakup fraction is

$$f_{\mathrm{BF}}^{(n/p)} = f_{\mathrm{BU}}^{(n/p)} - f_{\mathrm{EB}}, \quad (3)$$

and the corresponding inelastic-breakup cross sections, under the assumption that the BF cross section for neutron emission σ_{BF}^{n} is equal to that for the proton emission σ_{BF}^{p},

$$\sigma_{\mathrm{BF}}^{n/p} = f_{\mathrm{BF}}^{(n/p)}\sigma_R. \quad (4)$$

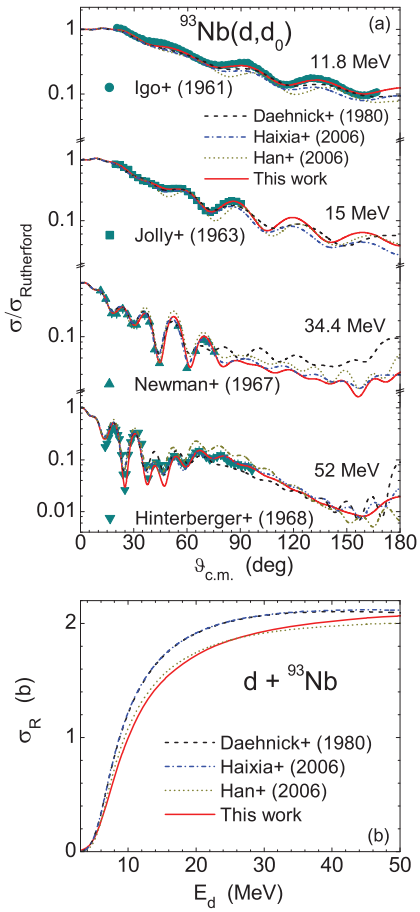

FIG. 1. (Color online) Comparison of (a) measured [21] deuteron elastic-scattering angular distributions for the ^{93}Nb target nucleus and calculated values using the OMP parameters given in Table IV (solid curves), previous optical potentials [26] (dashed curves), [27] (dash-dotted curves), and [28] (dotted curves), and (b) the corresponding total reaction cross sections.

A comparison of the above quantities could be made only to the total proton- and neutron-emission breakup cross-section parametrization of Kalbach [33],

$$\sigma_{\rm BU}^{n/p} = K_{d,n/p}\frac{(A^{1/3}+0.8)^2}{1+\exp\frac{(13-E)}{6}}, \quad K_{d,p}=21, \quad K_{d,n}=18, \quad (5)$$

TABLE IV. The parameters of the deuteron optical potential [23] for the ^{93}Nb target nucleus. A superscript asterisk follows the unchanged OMP parameters of Daehnick *et al.* [26].

Potential depths (MeV)	Geometry parameters (fm)
$V_R^* = 88.5{+}0.88Z/A^{1/3}{-}0.26E$	$r_R = 1.223{-}0.00155E$, $E < 34.4$
	$= 1.17^*$, $E > 34.4$
	$a_R = 0.671 + 0.0025E$, $E < 47.5$
	$= 0.709 + 0.0017E$, $E > 47.5^*$
$W_V = -1 + 0.114E$	$r_V = 1.28$, $a_V = 0.742$
$W_D = 15.7 - 0.118E$,	$r_D = 1.28$, $a_D = 0.682 + 0.003E$
$V_{\rm SO}^* = 7.33 - 0.029E$	$r_{\rm SO}^* = 1.07$, $a_{\rm SO}^* = 0.66$

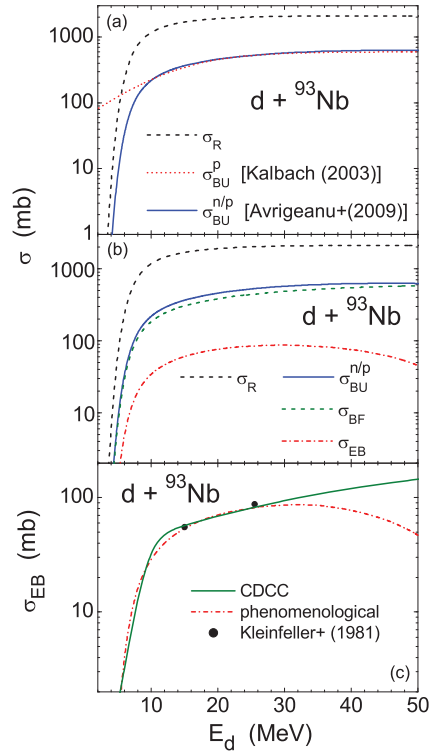

FIG. 2. (Color online) The energy dependence of (a) the deuteron total reaction cross section (dashed curves) and total breakup cross sections given by parametrizations of Avrigeanu *et al.* [4] (solid curve) and Kalbach [33] (dotted curve) for deuteron interactions with the ^{93}Nb target nucleus, (b) the BF (dashed curve) and EB (dash-dotted curve) breakup components [4], and (c) the comparison of the empirical [4] (dash-dotted curve) and CDCC [17] (solid curve) EB cross sections and values of Kleinfeller *et al.* [31] systematics (solid circles).

which is shown in Fig. 2(a) for the target nucleus ^{93}Nb. Regardless of the differences between them below the deuteron incident energy of 7 MeV, the two parametrizations are in good agreement.

Concerning the energy dependence of the EB and BF components [Fig. 2(b)], the interest on deuteron activation cross sections for incident energies up to 50 MeV motivated an additional check [17] for extension of the EB parametrization beyond the energies formerly considered for the derivation of its actual form. Actually, the parametrization for the elastic–breakup was obtained through analysis of the empirical systematics that covers an incident energy range from 15 to only 30 MeV [4]. However, as shown in Fig. 2(c) for the ^{93}Nb target nucleus, the corresponding EB cross-section decrease with the incident-energy increase beyond the energy range within which it was established, while the total-breakup cross section has an opposite trend. Therefore, in the absence of available experimental deuteron elastic-breakup data at incident energies above 30 MeV, the correctness of an eventual extrapolation should be checked by comparison of the related predictions with results of a theoretical model as, e.g., the continuum-discretized coupled-channels (CDCC) method [34–37].

The EB component has been considered within the CDCC formalism as an inelastic excitation of the deuteron, coupling its unbound excited states in the solution of the scattering problem within the coupled-channels approach [17]. In order to deal with a finite set of coupled equations, the *binning* method [34,35] has been used. The energy dependence of the EB cross sections provided in the case of the deuteron interaction with ^{93}Nb target nucleus by the excitation of the continuum spectrum (e.g., the population of the virtual excited states) is compared with the prediction of empirical systematics [4] in Fig. 2(c) too. The calculations were performed with the coupled-channels code FRESCO [13]. The EB cross sections corresponding to the Kleinfeller *et al.* systematics (Table III of Ref. [31]) are also shown. The agreement of the CDCC elastic-breakup cross sections [17] and the latter systematics can be considered as a validation of the present advanced model approach. Moreover, this comparison points out that the CDCC calculations lead to EB cross sections that follow the total-breakup cross-section behavior and shows that extrapolation of the empirical parametrization for the EB cross sections should be done with caution beyond the energies considered formerly in this respect [17].

B. BF enhancement of the deuteron activation cross sections

A similar consideration should be given to (i) the breakup process decreasing the total reaction cross section that is shared among different outgoing channels and (ii) the additional contributions to different reaction channels due to interactions of inelastic-breakup nucleons with the target nucleus. While the former effect has been taken into account by using a reduction factor $(1 - \sigma_{\rm BU}/\sigma_R)$ of the deuteron total reaction cross section, an enlarged discussion concerns the latter one.

The inelastic-breakup proton or neutron that interacts with the target nucleus at once with emission of a corresponding neutron or proton, respectively, contributes through a reaction (p, x) or (n, y) to the enhancement of the $(d, n + x)$ or $(d, p + y)$ reaction cross section. In order to calculate these BF enhancements, first, the BF cross section was obtained, for a given deuteron incident energy E, by subtracting the EB cross section from the phenomenological BU cross section. Next, the enhancement of, e.g., the $(d, n + x)$ reaction channel, is given by this BF cross section multiplied by the convolution of the ratio $\sigma_{(p,x)}/\sigma_R^p$ and Gaussian line-shape distribution of the BF-proton energies E_p [33,38] for the given deuteron incident energy. The enhancement of the $(d, p + y)$ reaction channel is obtained in a similar way but using the convolution of the

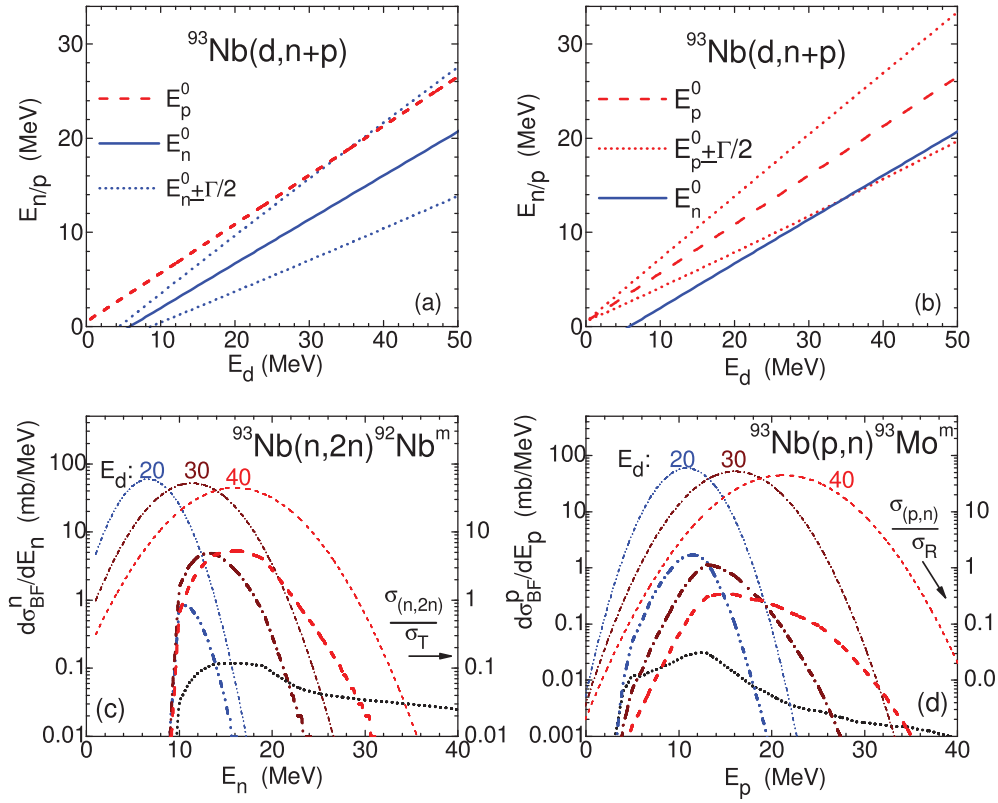

FIG. 3. (Color online) [(a) and (b)] The centroid of assumed Gaussian line shape [33,38] for deuteron breakup-peak energies of emitted neutrons (solid line) and protons (dashed line), and the corresponding $E \pm \Gamma/2$ values (dotted lines) for the BU (a) neutrons and (b) protons, calculated for deuterons interacting with ^{93}Nb. [(c) and (d)] The convolution of the cross-section ratios (c) $\sigma_{(n,2n)}/\sigma_T$ and (d) $\sigma_{(p,n)}/\sigma_R^p$ for the target nucleus ^{93}Nb, leading to residual-nucleus isomeric states (dotted curves), with the Gaussian line shape of the deuteron-breakup peak energies of the corresponding emitted (c) neutrons and (d) protons, for deuterons with energies of 20, 30, and 40 MeV (thin dash-dot-dotted, dash-dotted, and dashed curves, respectively, with the incident energy noted above their maxima) and the convolution results at each deuteron energy (thick curves).

ratio $\sigma_{(n,y)}/\sigma_T$ and Gaussian line-shape distribution of the BF-neutron energies E_n [33] for the given deuteron incident energy. The quantities σ_R^p and σ_T are the proton total reaction cross section and the neutron total reaction cross section, respectively, for the ^{93}Nb target nucleus. The quite large widths Γ of the assumed Gaussian line shape of these energies make necessary the improved estimation of the BF enhancement. These widths are shown for the deuteron BU on ^{93}Nb in Figs. 3(a) and 3(b). The corresponding Gaussian distributions of BF neutrons and protons energies, at several deuteron incident energies (20, 30, and 40 MeV), are shown together with the above-mentioned ratios for the particular reactions $(n, 2n)$ and (p, n), respectively, in Figs. 3(c) and 3(d). There are also shown the convolution results at each of these energies, while their area corresponds to the BF enhancement of the $(d, 2np)$ and $(d, 2n)$ reaction cross sections, respectively.

V. ONE-NUCLEON TRANSFER REACTIONS

Apart from the breakup contributions to deuteron interactions, increased attention is paid to direct reactions that have been very poorly accounted so far in deuteron activation analysis. For energies below and around the Coulomb barrier, the interaction of deuterons with target nuclei proceeds largely through DR mechanism, while PE and CN processes become more important with the incident energy increase. Thus, the DR stripping and pick-up are important for the increasing side of the (d, p), (d, n), and (d, t) excitation functions [4–9]. These processes have been considered in the frame of the CRC formalism by using the code FRESCO [13], with the post/prior form distorted-wave transition amplitudes for $(d, n/p)$, and, respectively, (d, t) reactions, and finite-range interactions. The n-p interaction in deuteron [34] as well as the d-n interaction in triton [39] are assumed to have a Gaussian shape, while the transferred nucleon bound states were generated in a Woods-Saxon real potential. The deuteron optical potential from Sec. II has been used in the incident channel, while Koning and Delaroche [40] and Becchetti and Greenlees [41,42] OMPs have been used for outgoing nucleon and triton channels, respectively.

Actually, the one-nucleon transfer reactions have been of critical importance for the nuclear structure studies, the spectroscopic factors extracted from the analysis of emitted particle angular distributions contributing to validation of the nuclear shell model. Consequently, the rich systematics of the achieved experimental spectroscopic factors makes possible the calculation of stripping and pick-up cross-section contributions to the deuteron activation. Thus, in the present analysis of deuteron interactions with the ^{93}Nb target nucleus, spectroscopic factors reported by Moorhead and Moyer [43] and Bhatia *et al.* [44] were used in the cross-section calculations for the ^{93}Nb$(d, p)^{94}$Nb and ^{93}Nb$(d, t)^{92}$Np reactions, respectively.

A particular note should concern the pick–up contribution to the total (d, t) activation cross section, usually neglected in spite of its essential contribution at the energies between its threshold and those for the (d, nd) and $(d, 2np)$ reactions that lead to the same residual nucleus. Thus, it will be shown in Sec. VII that the pick-up component of the (d, t) excitation function is critical for the description the experimental data at deuteron incident energies lower than 10 MeV, where other mechanism contributions (PE, CN) are almost negligible.

VI. PRE-EQUILIBRIUM AND COMPOUND NUCLEUS DECAY

The PE and CN reaction mechanisms concerning the statistical emission at pre-equilibrium or from the fully equilibrated compound nucleus become important when the incident energy is increased well above the Coulomb barrier. The related cross sections have been analyzed in this work by using the PE + CN code STAPRE-H [14] and local consistent parameters that have been obtained or checked through the analysis of various independent experimental data in advance to obtain the deuteron-activation cross sections for ^{93}Nb. The main assumptions and parameters involved in this work have recently been described elsewhere [7,45–47], so only some specific issues to the mass range $A \geqslant 90$ are given here. A further note should concern the fact that similar input parameters and calculations have been used to obtain the BF enhancement as discussed in Sec. VII.

The phenomenological OMP given in Table IV has been used for the incident channel. Concerning the nucleon optical potentials, the best description of the particular s- and p-wave neutron strength functions, the potential scattering radius R' [42], and the energy dependence of the total cross sections for the Mo isotopes [22] as well as the proton total reaction cross sections of the ^{93}Nb target nucleus [22] was obtained using the local neutron and proton OMP of Reimer *et al.* [45]. These potentials were also used for the calculation of the collective inelastic scattering cross sections that are also needed in the analysis of the nucleon-induced reactions on the target nucleus ^{93}Nb, which are of interest both for (i) check of the consistent input parameter set and (ii) estimation of the BF enhancement due to one of deuteron constituents interacting with the target nucleus. The direct-interaction distorted-wave Born approximation (DWBA) method and a local version of the computer code DWUCK4 [48] have been involved in this respect. The weak coupling model was adopted for the odd nucleus ^{93}Nb using the collective state parameters of Kalbach [49]. Typical ratios of the neutron direct inelastic scattering to the total reaction cross sections in the energy range from few to 60 MeV decrease from ∼11 to 5% [45]. An overall check of the nucleon OMPs and γ-ray transmission coefficients used in this work has been carried out by a simultaneous comparison of the calculated and measured cross sections for the reactions ^{93}Nb$(p, \gamma)^{94}$Mo and ^{93}Nb$(p, n)^{93}$Mo, available up to an incident energy of 5.5 MeV [50,51] (Fig. 4). The proton total reaction cross sections is also shown, being almost identical to the (p, n) reaction cross section above the proton energy of 3 MeV.

The optical potential which is used in this work for calculation of the α-particle transmission coefficients was established previously [52] for emitted α particles and supported recently by semimicroscopic analysis for $A \sim 90$ nuclei [53]. The same OMP parameter sets were also employed for calculation of the

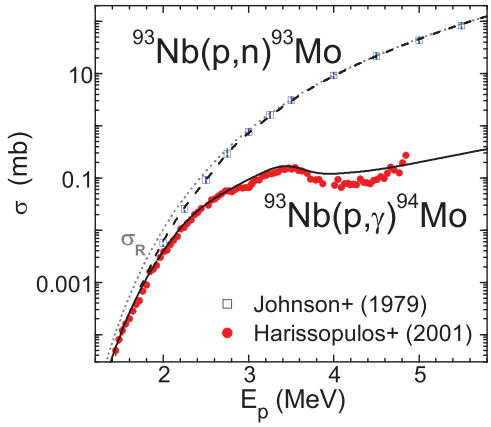

FIG. 4. (Color online) Comparison of the measured [50,51] and calculated cross sections for the reactions ^{93}Nb$(p,\gamma)^{94}$Mo (solid curve) and ^{93}Nb$(p,n)^{93}$Mo (dashed curve), respectively, by means of the nucleon OMPs and γ-ray transmission coefficients used in this work. The proton total reaction cross sections is also shown (dotted curve).

intranuclear transition rates within the PE generalized [14] geometry-dependent hybrid (GDH) model [54].

The nuclear level densities were derived on the basis of the back-shifted Fermi gas (BSFG) formula [55] for the excitation energies below the neutron-binding energy. The corresponding parameters a and Δ were obtained by a fit of the most recent experimental low-lying discrete levels [56] and s-wave nucleon resonance spacings D_0 [42] (Table V). For nuclei without resonance data we applied the smooth-curve method [57] by using average a values for the $A \sim 90$ and Δ values obtained by a fit of the low-lying discrete levels. Above the neutron binding we took into account the washing out of shell effects within the approach of Ignatyuk *et al.* [58] and Junghans *et al.* [59], while the method of Koning and Chadwick [60] was used to fix the appropriate shell correction energy. A transition range from the BSFG formula description to the higher-energy approach has been chosen between the neutron binding energy and the excitation energy of 15 MeV, mainly in order to have a smooth connection. On the other hand, the spin distribution has been determined using a variable ratio I/I_r of the nuclear moment of inertia to its rigid-body value, between 0.5 for ground states, 0.75 at the neutron binding energy, and 1 around the excitation energy of 15 MeV [61].

The basic role of the level density spin distribution for the model calculations of isomeric cross sections ([62] and references therein), which are the dominant deuteron activation measured data on ^{93}Nb, motivated a particular concern in this work. Thus, the current assumption for the moment of inertia is compared in Fig. 5 with other actual formulas of the level density spin cutoff σ^2 for the ^{93}Mo nucleus. Actually, this nucleus has a well-known isomeric level $21/2^+$ at the excitation energy of 2.425 MeV, with a large amount of measured isomeric cross sections through the ^{93}Nb$(d,2n)$ as well as ^{93}Nb(p,n) and ^{94}Mo$(n,2n)$ reactions. The additional forms that were considered in this respect are the usual alternate rigid-body and half rigid-body moments of inertia, the discrete spin cutoff σ_d^2 for the range of levels given in Table V for ^{93}Mo as well its energy dependence for higher energies of Koning *et al.* [63], and the latest energy-dependent parametrization of Eq. (6) in Ref. [64]. Also shown is the energy-dependent spin cutoff $\sigma^2(E_d^*)$ given by the maximum likelihood estimator, following the discussion in Ref. [65], namely the ratio of the sum of $(J_i + 1/2)^2$ term for all discrete levels with $E_i^* < E_d^*$ to twice the number of these levels. It results in the variable ratio I/I_r [61] corresponding to suitable σ_d^2 values in the energy range of the discrete levels [63–65], close to the assumption of Koning *et al.* [63] at the neutron binding energy, and in agreement with theoretical predictions [66] at higher energies. These results are in line with the recent conclusion that former values $I < I_r$, obtained from isomeric cross-section analysis were artificial and resulted from the use of an improper PE spin distribution, namely the CN spin distribution [67].

The composite formula [68] was used within the GDH model for the particle-hole state density (PSD), including the PE spin distribution that was discussed by Feshbach *et al.* [69] and further detailed by Fu [70]. The α-particle state density $g_\alpha = A/10.36$ MeV^{-1} [71] has also been adopted. Similar single-particle level densities g were used for deuteron and triton PE but increased by factors of 2 and 4/3, respectively, with respect to the α particles. The most important PSD correction for the nuclear potential finite-depth was obtained by using the Fermi energy value $F = 37$ MeV [72]. The FG energy dependence was adopted for the single-particle level densities of PE-excited particles and holes.

The recent high-accuracy measurements of the electric-dipole radiative strength function (RSF), of main importance for calculation of the γ-ray transmission coefficients, definitely pointed out a low-energy enhancement [73,74] not yet consistently described by models. Considering its importance for the isomeric cross-section calculation, an enhanced generalized Lorentzian model (EGLO) has been adopted in the present work for the electric dipole γ-ray strength functions $f_{E1}(E_\gamma)$. It is based, beyond the standard Lorentzian model (SLO) using the giant dipole resonance (GDR) line shape with the usual parameters (σ_{E1}, Γ_{E1}, and E_{E1}) derived from photoabsorption data, on the generalized Lorentzian model (GLO) form of Kopecky and Uhl [75] that included also a temperature dependence of the already energy-dependent GDR width [14,76,77]. While the GLO model was able to avoid the extrapolation of the SLO function in the limit of zero γ-ray energy, it provided a rather constant nonzero limit but no enhancement at energies below ~3 MeV [73,74]. We have followed Larsen and Goriely [78] and considered the modified width of the GLO model with an additional E_γ^{-1} dependence of its temperature dependence,

$$\Gamma(E_\gamma, T_f) = \frac{\Gamma_{E1}}{E_{E1}^2}\left[E_\gamma^2 + \frac{4\pi^2 T_f^2 E_{E1}}{(E_\gamma + \delta)}\right], \qquad (6)$$

where T_f is the nuclear temperature of the final states and the constant parameter $\delta = 0.05$ MeV was applied to ensure a finite RSF value at $E_\gamma = 0$. A constant temperature $T_f = 0.16$ MeV has been chosen formerly [78] to reproduce the experimental RSF of molybdenum isotopes [73], while recently a value $T_f = 0.5$ MeV has been used in

TABLE V. Low-lying level number N_d up to excitation energy E_d^* [56] used in cross-section calculations, and the levels and s-wave neutron-resonance spacings $D_0^{\rm exp}$ [42] in the energy range ΔE above the separation energy S, for the target-nucleus ground-state spin I_0, fitted to obtain the BSFG level-density parameter a and ground-state shift Δ, for a spin cutoff factor calculated with a variable moment of inertia between half and 75% of the rigid-body value from the ground state to S and reduced radius $r_0 = 1.25$ fm.

Nucleus	N_d		Fitted level and resonance data						
		E_d^* (MeV)	N_d	E_d^* (MeV)	$S+\frac{\Delta E}{2}$ (MeV)	I_0	$D_0^{\rm exp}$ (keV)	a (MeV^{-1})	Δ (MeV)
^{84}Sr	25	3.332	25	3.332				9.60	0.95
^{85}Sr	27	1.712	26	1.701	8.532	0	0.32 ± 0.12	10.64	−0.46
^{86}Sr	29	3.501	29	3.501				9.10	0.83
^{87}Sr	39	2.940	39	2.940	8.442	0	2.6 ± 0.8	9.15	0.07
^{88}Sr	33	4.614	33	4.614	11.113	9/2	0.29 ± 0.08	8.75	1.70
^{89}Sr	18	3.073	39	2.940	6.430	0	23.7 ± 2.9	9.48	0.79
^{86}Y	21	1.277	21	1.277				9.40	−1.12
^{87}Y	24	1.847	24	1.847				9.50	−0.57
^{88}Y	24	1.477	24	1.477				9.40	−1.00
^{89}Y	30	3.660	25	3.515				9.50	1.06
^{90}Y	17	1.815	15	1.761	6.857	1/2	3.7 ± 0.4	9.23	−0.46
^{87}Zr	24	1.949	24	1.949				9.15	−0.58
^{88}Zr	18	3.060	18	3.060				8.75	0.62
^{89}Zr	22	2.280	22	2.280				9.40	−0.11
^{90}Zr	38	4.783	38	4.783				8.50	1.68
^{91}Zr	31	2.928	31	2.928	7.260	0	6.0 ± 1.4	10.10	0.48
^{92}Zr	42	3.500	42	3.500	8.647	5/2	0.55 ± 0.10	9.60	0.71
^{93}Zr	21	2.095	21	2.095	6.785	0	3.5 ± 0.8	10.50	−0.02
^{89}Nb	20	2.221	20	2.221				9.40	−0.12
^{90}Nb	17	1.195	17	1.195				9.20	−1.17
^{91}Nb	24	2.413	24	2.413				9.60	0.00
^{92}Nb	25	1.566	22	1.473				10.00	−0.80
^{93}Nb	24	1.500	24	1.500				9.90	−0.85
^{94}Nb	33	1.086	33	1.086	7.232	9/2	0.094 ± 0.010	10.90	−1.24
^{90}Mo	22	3.185	22	3.185				9.20	1.17
^{91}Mo	21	2.451	21	2.451				9.30	−0.08
^{92}Mo	33	3.964	34	4.019				9.60	1.35
^{93}Mo	58	2.915	58	2.915	8.092	0	2.7 ± 0.5	9.35	−0.18
^{94}Mo	60	3.462	60	3.462				10.70	0.77
^{95}Mo	27	1.692	27	1.692	7.377	0	1.32 ± 0.18	10.40	−0.61

large-scale calculations [79]. However, unlike them, we have assumed the usual temperature formula [75] but with the rotational energy subtracted from the excitation energy. The results obtained for the ^{93,94,95}Mo isotopes, of interest for the present work, reproduce not only the experimental RSF low-energy enhancement but also the absolute values without any normalization (Fig. 6). The RSF values for $E1$ radiations that are obtained by normalization of the corresponding s-wave average radiative widths $\langle\Gamma_\gamma\rangle$ to experimental data [42] are also shown in Fig. 6, while SLO strength functions were used for $M1$ radiations [75] and global estimations [57] for multipoles $\lambda \leqslant 3$.

These RSF values have also been checked within the above-mentioned calculations of the ^{93}Nb$(p,\gamma)^{94}$Mo capture cross sections in the proton energy range between 1.4 and 5 MeV by using the OMP and nuclear level density parameters described above, with the results shown in Fig. 4. The agreement with the experimental data [50] is very good up to an energy of 3.7 MeV while the structure above this incident energy has been proved to be independent by the adopted RSF and level densities (Fig. 9 of Ref. [80]).

No free parameter is formally involved for the nucleon PE description within the generalized GDH model except for the α-particle preformation probability [71] $\varphi = 0.25$. The same approach has been adopted for deuteron and triton PE, with the preformation probabilities of 0.5 and 0.25, respectively, following the ratio of their mass to that of an α particle. These assumptions were supported finally by the agreement between the calculated and measured reaction cross sections. Moreover, a particular comment should concern the initial configuration of excited particles (p) and holes (h) for deuteron-induced reactions. Similar careful studies [31,32,81,82] pointed out that 3p-1h or 2p-1h may be a suitable choice for this configuration. Our calculations in the present work show that the former one gives the best agreement between the measured and calculated reaction cross sections.

VII. RESULTS AND DISCUSSION

All above reaction mechanisms and model parameters have been consistently used for calculation of the

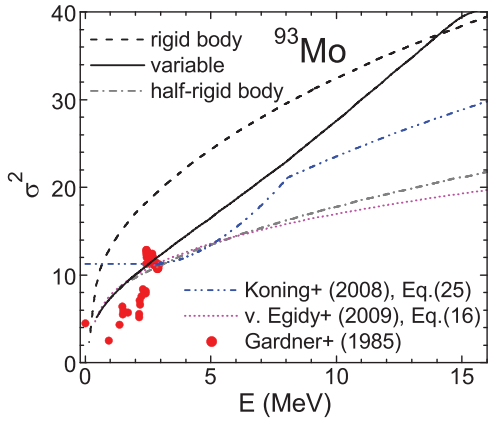

FIG. 5. (Color online) The excitation-energy dependence of the level density spin cutoff for the nucleus ^{93}Mo, corresponding to the rigid-body (dashed curve), half-rigid-body (dash-dotted), and variable [61] (solid curve) moment of inertia, the discrete value for the range of levels given in Table V for ^{93}Mo as well the energy-dependent form at higher energies of Koning *et al.* [63] (dash-dot-dotted curve), the energy-dependent parametrization of Ref. [64] (dotted curve), and the maximum likelihood estimator [65] (solid circles).

deuteron-activation cross sections of ^{93}Nb that can be compared to available measured data. The total reaction cross section given by the OMP parameter in Table IV was first reduced by the sum of BU and DR cross sections. It then was used to obtain the total PE cross section that was furthermore also subtracted from σ_R before the CN calculations. The CN contributions to a residual nucleus, eventually via different reaction channels, to finally complete the activation cross section of the respective nucleus. The consistency of the local input parameters and the unitary consideration of the BU, DR, PE, and CN mechanisms should make possible a suitable description of all available experimental data for various reaction channels of the deuteron interaction with the target nucleus ^{93}Nb (Fig. 7). Actually the same approach should provide a similar agreement also for different incident reaction channels leading to activation of the same residual nuclei. This last point is, however, beyond the object of this work except brief remarks, while the degree of reaching the former goal is discussed in the following.

Calculations for the same reactions were also performed by means of either the default model parameters or a particular set of options of the code TALYS (Fig. 8). The comparison of local and global predictions, the former being obviously more accurate, is, however, twofold: (i) to check unexpected differences between measured and calculated cross sections and (ii) to estimate the current precision of the global predictions with reference to the local analysis that is obviously superior but resource consuming.

A. The local analysis

The comparison of the measured and calculated activation cross sections is shown in Fig. 7, including the contributions of each reaction mechanism. The deuteron inelastic-breakup enhancement of the corresponding reaction cross sections is shown by curves identified with the BF mark, while the

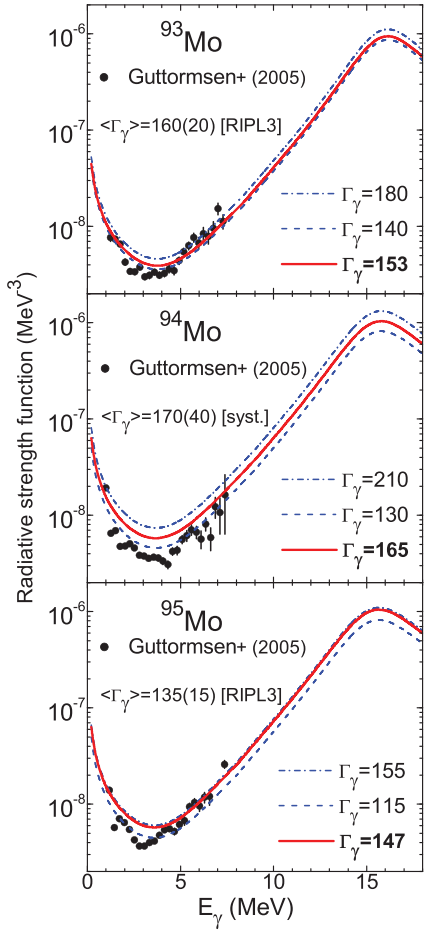

FIG. 6. (Color online) Comparison of measured [73] and non-normalized calculated EGLO strength functions for $E1$ radiations (solid curves) for the ^{93,94,95}Mo isotopes. The RSF obtained by normalization of the corresponding s-wave average radiative widths $\langle\Gamma_\gamma\rangle$ (in meV) to the lower (dashed curves) or upper (dash-dotted curves) limits of the measured data [42], for ^{93,95}Mo, or estimated from systematics [73], for ^{94}Mo, are also shown.

decrease of the deuteron total reaction cross section due to the whole BU process affects all subsequent reaction channels and mechanisms. This is the reason for using the mark BU rather than BF for the sum of various contributions to an activation cross section.

The ^{93}Nb$(d, p)^{94}$Nb^m *reaction* is well described above the incident energy of ∼10 MeV. The DR mechanism, discussed in Sec. V, is by far the dominant mechanism for this reaction. The PE + CN contribution is lower by nearly one order of magnitude while the BU enhancement decreases with another similar order, so they may have no effect, especially at the lower energies, on account of the measured data. Additional investigation of this discrepancy seems, therefore, to be needed. One may note that the analysis of the alternate incident channel, i.e., the ^{94}Mo$(n, p)^{94}$Nb^m reaction [45], did not face any problem but it benefited by only a few measured data around the incident energy of 14 MeV while its CN-dominant mechanism markedly differs.

The ^{93}Nb$(d, 2n)^{93}$Mo^m *reaction* represents a completely different case, with the BF contribution being, up to the

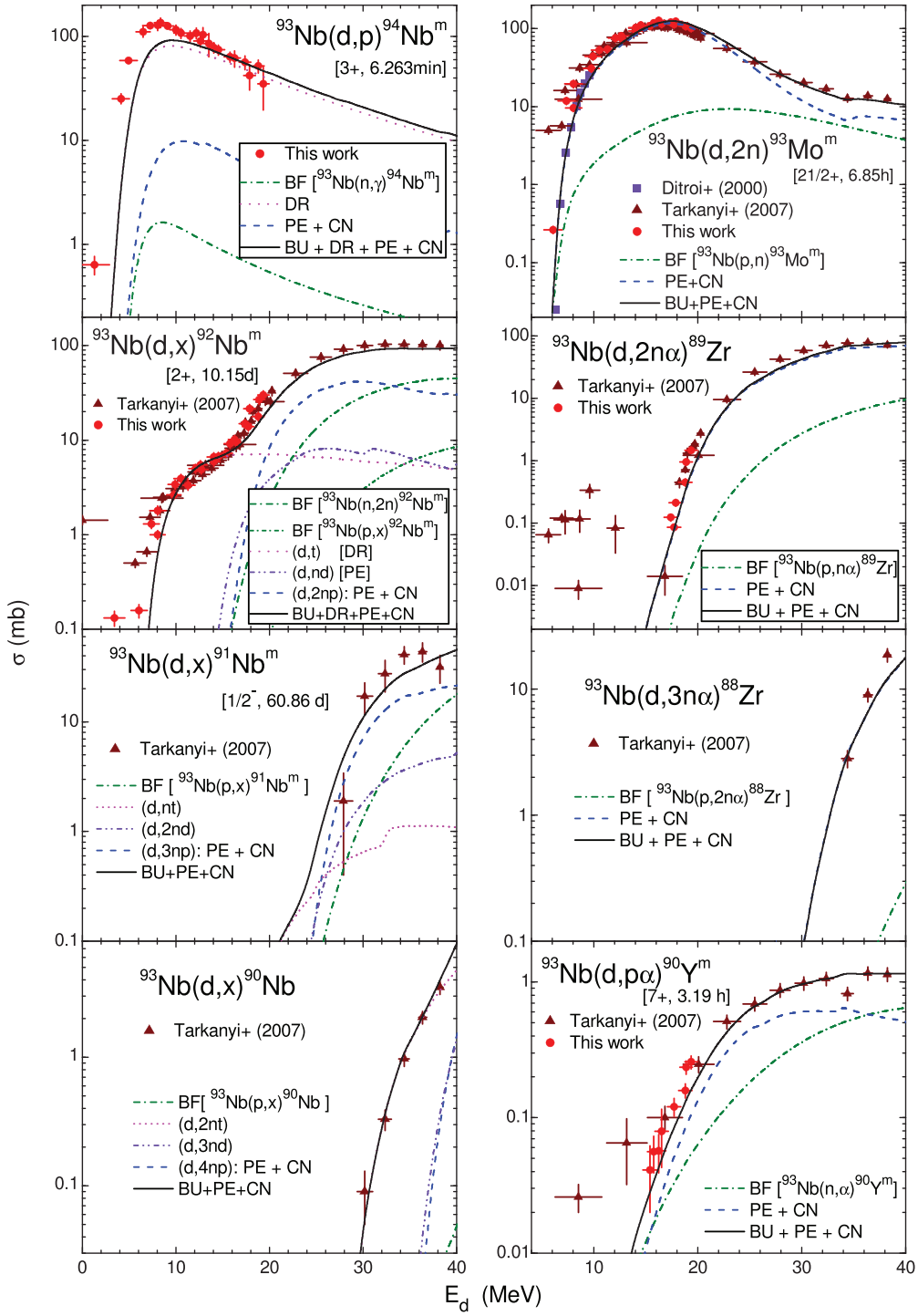

FIG. 7. (Color online) Comparison of previous [11,12] and measured deuteron activation cross sections of ^{93}Nb in this work (solid circles) and the present analysis results (solid curves), taking into account various mechanism contributions, namely the deuteron inelastic-breakup enhancement (dash-dotted and short dash-dotted curves), the DR (dot curves), and the PE + CN (dashed curves) with particular emphasis of the (d, xnd) (dash-dot-dotted curves) and (d, xnt) (short dashed) reactions, where $x = 1$–3.

deuteron energy of ∼20 MeV, again more than an order of magnitude lower than the statistical emission fully at equilibrium. However, since the BF contribution to the reaction cross section comes through the ^{93}Nb$(p, n)^{93}$Mo^m reaction, this contribution increase up to nearly 50% above the deuteron energy of ∼32 MeV. Overall, the agreement of the calculated and measured data is very good in the whole energy range, with a key role of the BF enhancement at deuteron higher energies.

A particular note should concern the well-known isomeric level $21/2^+$ at the excitation energy of 2.425 MeV in the ^{93}Mo residual nucleus. While the particular discussion in

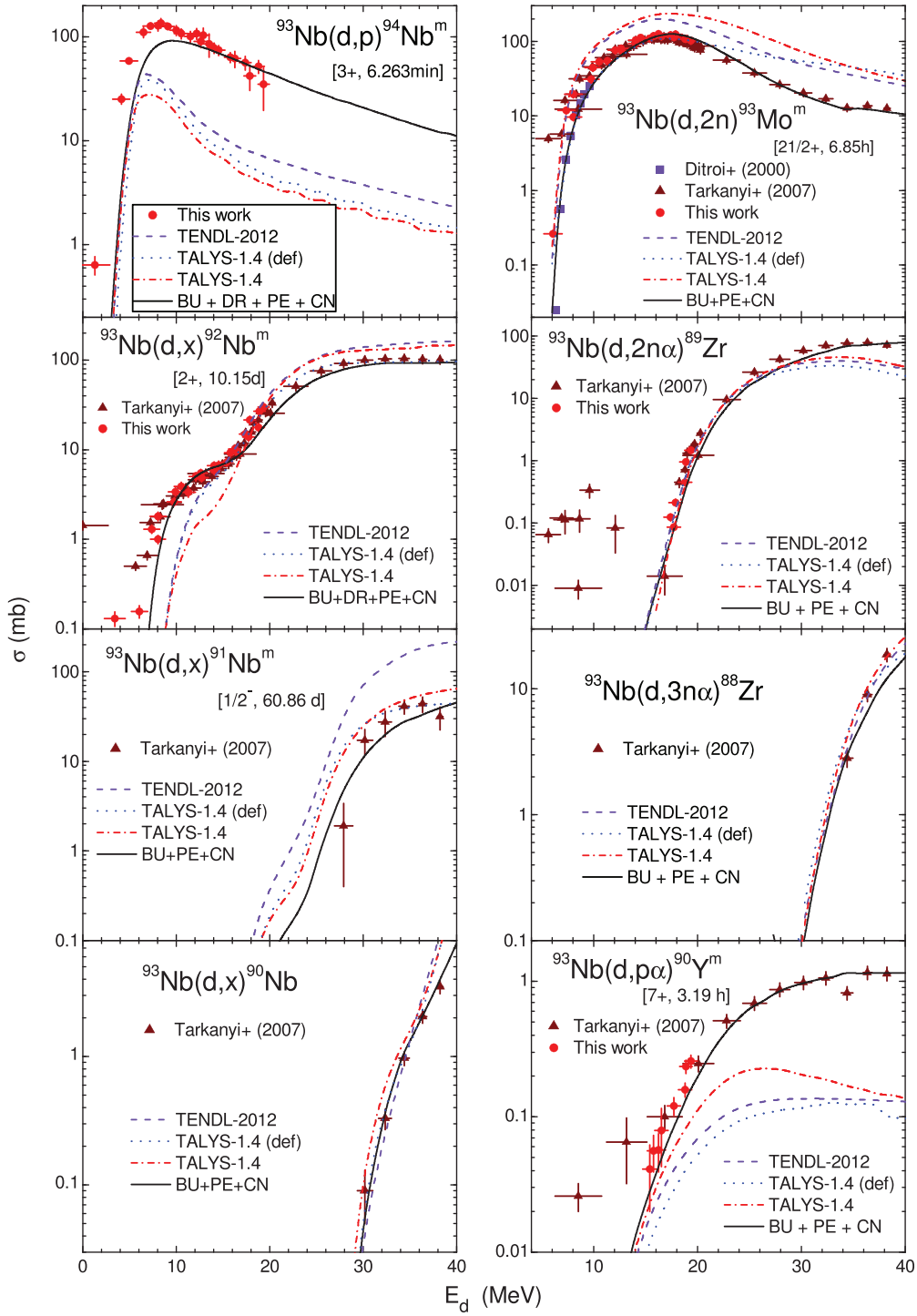

FIG. 8. (Color online) Comparison of measured data already shown in Fig. 7, the present analysis results (solid curves), evaluated data within the TENDL-2012 library [16] (dashed curves), and calculated results obtained with TALYS-1.4 code using either the whole default input (dotted curves) or the particular options mentioned in the text (dash-dotted curves).

Sec. VI on the current assumption for the moment of inertia concerned just this nucleus (Fig. 5), the large amount of measured isomeric cross sections for the ^{94}Mo$(n, 2n)^{93}$Mo^m reaction has already been well described by using rather the same approach and parameter set [45]. We have also obtained a similar good description of the ^{93}Nb$(p, n)^{93}$Mo^m reaction excitation functions to form the subject of another paper. One may consider this fact as sound support for the actual option adopted for the nuclear moment of inertia.

The ^{93}Nb$(d, x)^{92}$Nb^m *reaction* is the most interesting one from the point of view of various contributing reaction mechanisms. It takes place fully through the pick-up reaction

(d, t) at deuteron energies lower than the effective thresholds for emission of two to three particles, namely below ∼15 MeV. The DR character then becomes insignificant, contributing less than an order of magnitude at incident energies above 20 MeV. A similar case is that of the (d, nd) reaction contribution following by far the deuteron PE. On the other hand, there are two different BF contributions, through the ^{93}Nb$(n, 2n)^{92}$Nb^m and ^{93}Nb$(p, n)^{92}$Nb^m BF nucleon-induced reactions. The former contribution is obviously larger by a factor of ∼5 than the latter, but more worthy of note is its interplay with the PE + CN contribution of the $(d, 2np)$ reaction. Both of them have a similar effective threshold around 16 MeV, and then PE + CN increases faster and becomes twice as large around 24 MeV but begins to decrease after reaching its maximum around 29 MeV. Thus, the BF contribution is already the dominant one above the incident energy of 33 MeV. Altogether, the agreement of the sum of five contributions and the measured data is rather good except for the data below even the (d, t) reaction effective threshold.

The ^{93}Nb$(d, p\alpha)^{90}$Y^m *reaction* is rather similar concerning the interplay of the BF, through the ^{93}Nb$(n, \alpha)^{90}$Y^m reaction, and the PE + CN contributions. They have effective thresholds around 14 MeV, and then PE + CN increases faster and becomes twice as large around 25 MeV. However, since it decreases above ∼34 MeV, the BF contribution again becomes the dominant one above ∼37 MeV. The suitable description of this isomeric cross sections is particularly of interest due to the different case of the relation between the ground state and isomeric state spins, for the two residual nuclei ^{90}Y and ^{92}Nb that have proton number below and respective above the semimagic number 40. Thus, the former nucleus has a high-spin isomer while a low-spin value stands for the latter isomer. The suitable description of these both excitation functions validates once more the moment of inertia assumed for the nuclear level density spin distribution.

The ^{93}Nb$(d, x)^{91}$Nb^m *reaction* marks the limit of the number and type of emitted particles for which the BF enhancement is yet significant. It proceeds as the PE + CN contribution of the $(d, 3np)$ reaction. Furthermore, this contribution remains lower by a factor of ∼5, at the highest energy of the available experimental data, for the other reactions that are discussed below.

The ^{93}Nb$(d, 2n\alpha)^{89}$Zr *reaction* corresponds to a residual nucleus, for deuterons incident on ^{93}Nb, with larger total activation cross sections that can be measured. The agreement between the experimental and calculated cross sections is beyond the questions related to the accuracy of the spin-distribution description of the residual nucleus levels and may illustrate, first, the correctness of the α-particle optical potential [52].

The ^{93}Nb$(d, 3n\alpha)^{88}$Zr *reaction* may be considered as a case similar to the above one except the residual nucleus mass is smaller by one unit.

The ^{93}Nb$(d, x)^{90}$Nb *reaction* is a particular case with measured cross sections that are larger than both the $(d, 4np)$ and $(d, 3nd)$ contributions. The agreement finally obtained between the calculated and experimental data may support eventually the PE approach adopted for tritons, following the model of Gadioli [71] for α-particle PE.

B. The global predictions

Concerning the global predictions of the large-scale nuclear-model calculations with the code TALYS, the most immediate way has been to take into account the latest version of the evaluated data library TENDL-2012. Actually, it is based on both default and adjusted TALYS calculations on data from other sources [16]. The tabular residual cross sections in this library, corresponding to the available activation data for deuterons incident on ^{93}Nb, are compared in Fig. 8 with the local analysis results. There are activation cross sections for several residual nuclei that are in agreement with the measured data, e.g., for the $(d, 2n)$ reaction up to the incident energy of 20 MeV, $(d, 4np)$ including complex-particle emission, and $(d, 3n\alpha)$ reactions. On the other hand, the disagreement for the important channels (d, p), $(d, 2n)$ above 20 MeV, $(d, 2np)$ and $(d, 3np)$ including the corresponding complex-particle emission, and $(d, p\alpha)$ goes from factors of 2 to 5. Therefore, before drawing conclusions, we performed two runs of TALYS-1.4 calculations.

First, a TALYS calculation using its default input parameters was performed. Next, we adopted several particular options within a second calculation with TALYS. Thus, we chose the BSFG nuclear level density formalism and parameters, and the particular OMP parameter sets involved within the local approach of the present work except the case of deuterons. We adopted for the incident channel the potential of Daehnick *et al.* [26], available in TALYS and which provided results closer to the parameter set given in Table IV of the present work.

The calculated results obtained by these two runs are also shown in Fig. 8. In most cases they are close except for the reaction $(d, p\alpha)$, where an improvement by a factor of 2 around the maximum of the excitation function was obtained by using different options. A similar improvement was also found for this reaction with reference to the TENDL data, while even a factor of ∼5 was found in the same respect for the $(d, 3np)$ reaction. The largest discrepancies between the calculated and measured data remained finally for the basic reactions (d, p), $(d, 2n)$, and $(d, p\alpha)$, while closer local and global results have been obtained for reactions in which the BU effects are not significant, namely $(d, 3np)$, $(d, 3n\alpha)$, and $(d, 4np)$.

VIII. SUMMARY

Cross sections for deuteron-induced reactions on natural Nb were measured for the reactions (d, p), $(d, 2n)$, $(d, 2np + nd + t)$, $(d, 2n\alpha)$, and $(d, p\alpha)$ on ^{93}Nb at deuteron energies up to 20 MeV. They are in good agreement with the several previously reported experiments [11,12].

A consistent, energy-dependent, optical potential has been given for deuterons incident on ^{93}Nb. The deuteron breakup effects on ^{93}Nb activation data were established on this basis. Moreover, one-nucleon transfer DR analysis was carried out using the computer code FRESCO. A discussion of the local input parameter set involved in the PE and CN analysis using the code STAPRE-H [14] underlines the achievement of a suitable description of the spin distribution of nuclear level densities as well as the radiative strength functions.

All above reaction mechanisms and model parameters were consistently involved in calculation of the deuteron-activation cross sections of ^{93}Nb that can be compared to the measured data. The total reaction cross sections σ_R given by the OMP parameter set in Table IV were, first, reduced by the sum of BU and DR cross sections, and then the total PE cross section was obtained and furthermore subtracted from σ_R. The CN contributions to a residual nucleus, eventually via different reaction channels, finally complete the activation cross section of the respective nucleus. The consistency of the local input parameter set, established by analysis of various other independent data, as well as that of the unitary consideration of the BU, DR, PE, and CN mechanisms, made possible a suitable description of all available experimental data for various reactions induced by deuterons on ^{93}Nb. The local approach led to much better agreement with the present (d, p) reaction data, especially due to the model calculation that accounts for the DR stripping contribution. Moreover, consideration of the deuteron breakup plays a key role for the reaction channels adding a second emitted particle to the first one.

In completion of the local approach, based on the use of the codes FRESCO and STAPRE-H, similar calculations by means of either the default model parameters or a particular set of options of the widely used computer code TALYS were performed. All calculation results were compared with the evaluated data from the TENDL-2012 library. There are activation cross sections for several residual nuclei in agreement with the measured data, e.g., for $(d, 2n)$ reaction up to the incident energy of 20 MeV, $(d, 4np)$ including complex-particle emission, and $(d, 3n\alpha)$. On the other hand, the disagreement for the important channels (d, p), $(d, 2n)$ above 20 MeV, $(d, 2np)$ and $(d, 3np)$ including the corresponding complex-particle emission, and $(d, p\alpha)$ goes from factors of 2 to 5. The largest discrepancies between the calculated and measured data remained finally for the basic reactions (d, p), $(d, 2n)$, and $(d, p\alpha)$, while closer local and global results were obtained for reactions in which the BU effects are insignificant, namely $(d, 3np)$, $(d, 3n\alpha)$, and $(d, 4np)$.

ACKNOWLEDGMENT

This work was partly supported under the Karlsruher Institut für Technologie (KIT) Order No. 320/20504307/INR-NK and by a grant by the Romanian National Authority for Scientific Research, CNCS-UEFISCDI, Project No. PN-II-ID-PCE-2011-3-0450.

[1] http://www.iter.org/proj
[2] http://www.ifmif.org/b/
[3] http://pro.ganil-spiral2.eu/spiral2/instrumentation/nfs
[4] M. Avrigeanu, W. von Oertzen, R. A. Forrest, A. C. Obreja, F. L. Roman, and V. Avrigeanu, Fusion Eng. Des. **84**, 418 (2009).
[5] P. Bém, E. Šimečková, M. Honusek, U. Fischer, S. P. Simakov, R. A. Forrest, M. Avrigeanu, A. C. Obreja, F. L. Roman, and V. Avrigeanu, Phys. Rev. C **79**, 044610 (2009).
[6] M. Avrigeanu and V. Avrigeanu, Eur. Phys. J. Web Conf. **2**, 01004 (2010); J. Phys: Conf. Ser. **205**, 012014 (2010); E. Šimečková, P. Bém, M. Götz, M. Honusek, J. Mrázek, J. Novák, M. Štefánik, L. Závorka, M. Avrigeanu, and V. Avrigeanu, Eur. Phys. J. Web Conf. **8**, 07002 (2010).
[7] E. Šimečková, P. Bém, M. Honusek, M. Štefánik, U. Fischer, S. P. Simakov, R. A. Forrest, A. J. Koning, J. C. Sublet, M. Avrigeanu, F. L. Roman, and V. Avrigeanu, Phys. Rev. C **84**, 014605 (2011).
[8] M. Avrigeanu and V. Avrigeanu, J. Korean Phys. Soc. **59**, 903 (2011); E. Šimečková, P. Bém, M. Honusek, L. Závorka, U. Fischer, S. P. Simakov, R. A. Forrest, M. Avrigeanu, V. Avrigeanu, and F. L. Roman, *ibid.* **59**, 1928 (2011).
[9] M. Avrigeanu and V. Avrigeanu, Eur. Phys. J. Web Conf. **21**, 07003 (2012).
[10] M. Avrigeanu, V. Avrigeanu, and A. J. Koning, Phys. Rev. C **85**, 034603 (2012).
[11] F. Ditrói, F. Tarkányi, and M. A. Ali, Nucl. Instrum. Methods B **161–163**, 172 (2000).
[12] F. Tarkányi, A. Hermanne, F. Ditrói, S. Takács, B. Király, M. Baba, T. Ohtsuki, S. F. Kovalev, and A. V. Ignatyuk, Nucl. Instrum. Methods B **255**, 297 (2007).
[13] I. J. Thompson, Comput. Phys. Rep. **7**, 167 (1988); v. FRES 2.3 (2007).
[14] M. Avrigeanu and V. Avrigeanu, IPNE Report No. NP-86-1995, 1995, and references therein; News NEA Data Bank **17**, 22 (1995).
[15] A. J. Koning, S. Hilaire, and M. C. Duijvestijn, TALYS-1.0, as Ref. [25], p. 211; TALYS-1.4, December 2011 http://www.talys.eu
[16] A. J. Koning *et al.*, TENDL-2012: TALYS-based Evaluated Nuclear Data Library, accessed 11 January, 2013 http://www.talys.eu/tendl-2012/
[17] M. Avrigeanu and A. M. Moro, Phys. Rev. C **82**, 037601 (2010).
[18] M. Avrigeanu and V. Avrigeanu, in *Proc. 13th Int. Conf. on Nuclear Reaction Mechanisms, Varenna, Italy, 11–15 June 2012*, edited by F. Cerutti *et al.* (CERN, Geneva, 2012), p. 159.
[19] J. F. Ziegler, J. P. Biersack, and M. D. Ziegler, SRIM–*The Stopping and Range of Ions in Matter* (SRIM Co., Chester, MD, 2008); SRIM code http://www.srim.org
[20] S. Y. F. Chu, L. P. Ekström, and R. B. Firestone, The Lund/LBNL Nuclear Data, Search Version 2.0, February 1999 http://nucleardata.nuclear.lu.se/nucleardata/toi/
[21] G. Igo, W. Lorenz, and U. Schmidt-Rohr, Phys. Rev. **124**, 832 (1961); E. Newman, L. C. Becker, and B. M. Freedom, Nucl. Phys. A **100**, 225 (1967); R. K. Jolly, E. K. Lin, and B. L. Cohen, Phys. Rev. **130**, 2391 (1963); F. Hinterberger, G. Mairle, U. Schmidt-Rohr, G. J. Wagner, and P. Turek, Nucl. Phys. A **111**, 265 (1968).
[22] Experimental Nuclear Reaction Data (EXFOR) www-nds.iaea.or.at/exfor
[23] M. Avrigeanu, W. von Oertzen, U. Fischer, and V. Avrigeanu, Nucl. Phys. A **759**, 327 (2005).
[24] M. Avrigeanu, W. von Oertzen, H. Leeb, F. L. Roman, and V. Avrigeanu, in *Proc. 11th Int. Conf. on Nuclear Reaction Mechanisms, 12–16 June 2006, Varenna, Italy* (Ricerca Scientifica ed Educazione Permanente, Milano, 2006), p. 193.
[25] M. Avrigeanu, H. Leeb, W. von Oertzen, F. L. Roman, and V. Avrigeanu, in *Proc. Int. Conf. on Nuclear Data for Science and Technology, Nice, 2007*, edited by O. Bersillon *et al.* (EDP Sciences, Paris, 2008), p. 2192.

[26] W. W. Daehnick, J. D. Childs, and Z. Vrcelj, Phys. Rev. C **21**, 2253 (1980).
[27] Haixia An and Chonghai Cai, Phys. Rev. C **73**, 054605 (2006).
[28] Yinlu Han, Yuyang Shi, and Qingbiao Shen, Phys. Rev. C **74**, 044615 (2006).
[29] J. Bojowald, H. Machner, H. Nann, W. Oelert, M. Rogge, and P. Turek, Phys. Rev. C **38**, 1153 (1988).
[30] S. Watanabe, Nucl. Phys. **8**, 484 (1958).
[31] J. Kleinfeller, J. Bisplinghoff, J. Ernst, T. Mayer-Kuckuk, G. Baur, B. Hoffmann, R. Shyam, F. Rosel, and D. Trautmann, Nucl. Phys. A **370**, 205 (1981).
[32] J. Pampus, J. Bisplinghoff, J. Ernst, T. Mayer-Kuckuk, J. Rama Rao, G. Baur, F. Rosel, and D. Trautmann, Nucl. Phys. A **311**, 141 (1978); J. R. Wu, C. C. Chang, and H. D. Holmgren, Phys. Rev. C **19**, 370 (1979); N. Matsuoka, M. Kondo, A. Shimizu, T. Saito, S. Nagamachi, H. Sakaguchi, A. Goto, and F. Ohtani, Nucl. Phys. A **345**, 1 (1980); M. G. Mustafa, T. Tamura, and T. Udagawa, Phys. Rev. C **35**, 2077 (1987).
[33] C. Kalbach Walker, TUNL XLII Progress Report, 2003.
[34] M. Kawai, M. Kamimura, and K. Takesako, Prog. Theor. Phys. Suppl. **89**, 118 (1986).
[35] N. Austern, Y. Iseri, M. Kamimura, M. Kawai, G. Rawitscher, and M. Yahiro, Phys. Rep. **154**, 125 (1987).
[36] R. A. D. Piyadasa, M. Kawai, M. Kamimura, and M. Yahiro, Phys. Rev. C **60**, 044611 (1999).
[37] A. M. Moro and F. M. Nunes, Nucl. Phys. A **767**, 138 (2006); A. M. Moro, J. M. Arias, J. Gómez-Camacho, and F. Pérez-Bernal, Phys. Rev. C **80**, 054605 (2009); A. M. Moro, F. M. Nunes, and R. C. Johnson, *ibid.* **80**, 064606 (2009).
[38] C. Kalbach Walker, *1st Research Co-ordination Meeting of the Fusion Evaluated Nuclear Data Library FENDL 3.0, 2–5 December 2008, IAEA, Vienna* http://www-nds.iaea.org/fendl3/RCM1_documents.html
[39] P. Guazzoni, L. Zetta, A. Covello, A. Gargano, B. F. Bayman, T. Faestermann, G. Graw, R. Hertenberger, H.-F. Wirth, and M. Jaskola, Phys. Rev. C **83**, 044614 (2011).
[40] A. J. Koning and J. P. Delaroche, Nucl. Phys. A **713**, 231 (2003).
[41] F. D. Becchetti Jr., G. W. Greenlees, and J. H. Williams Laboratory, University of Minnesota, Annual Report, 1969.
[42] R. Capote *et al.*, Nucl. Data Sheets **110**, 3107 (2009) http://www-nds.iaea.org/RIPL-3/
[43] J. B. Moorhead and R. A. Moyer, Phys. Rev. **184**, 1205 (1969).
[44] T. S. Bhatia, W. W. Daehnick, and T. R. Canada, Phys. Rev. C **3**, 1361 (1971).
[45] P. Reimer, V. Avrigeanu, S. V. Chuvaev, A. A. Filatenkov, T. Glodariu, A. Koning, A. J. M. Plompen, S. M. Qaim, D. L. Smith, and H. Weigmann, Phys. Rev. C **71**, 044617 (2005).
[46] M. Avrigeanu, S. Chuvaev, A. A. Filatenkov, R. A. Forrest, M. Herman, A. J. Koning, A. J. M. Plompen, F. L. Roman, and V. Avrigeanu, Nucl. Phys. A **806**, 15 (2008).
[47] M. Avrigeanu and V. Avrigeanu, Phys. Rev. C **79**, 027601 (2009).
[48] P. D. Kunz, DWUCK4 user manual, OECD/NEA Data Bank, Issy-les-Moulineaux, France, 1984 www.nea.fr/abs/html/nesc9872.html
[49] C. Kalbach, Phys. Rev. C **62**, 044608 (2000).
[50] S. Harissopulos, E. Skreti, P. Tsagari, G. Souliotis, P. Demetriou, T. Paradellis, J. W. Hammer, R. Kunz, C. Angulo, S. Goriely, and T. Rauscher, Phys. Rev. C **64**, 055804 (2001).
[51] C. H. Johnson, A. Galonsky, and R. L. Kernell, Phys. Rev. C **20**, 2052 (1979).
[52] V. Avrigeanu, P. E. Hodgson, and M. Avrigeanu, Phys. Rev. C **49**, 2136 (1994).
[53] M. Avrigeanu, W. von Oertzen, and V. Avrigeanu, Nucl. Phys. A **764**, 246 (2006).
[54] M. Blann and H. K. Vonach, Phys. Rev. C **28**, 1475 (1983).
[55] H. Vonach, M. Uhl, B. Strohmaier, B. W. Smith, E. G. Bilpuch, and G. E. Mitchell, Phys. Rev. C **38**, 2541 (1988).
[56] Evaluated Nuclear Structure Data File (ENSDF) http://www.nndc.bnl.gov/ensdf/
[57] C. H. Johnson, Phys. Rev. C **16**, 2238 (1977).
[58] A. V. Ignatyuk, G. N. Smirenkin, and A. S. Tishin, Yad. Fiz. **21**, 485 (1975) [Sov. J. Nucl. Phys. **21**, 255 (1975)].
[59] A. R. Junghans, M. de Jong, H.-G. Clerc, A. V. Ignatyuk, G. A. Kudyaev, and K.-H. Schmidt, Nucl. Phys. A **629**, 635 (1998).
[60] A. J. Koning and M. B. Chadwick, Phys. Rev. C **56**, 970 (1997).
[61] V. Avrigeanu, T. Glodariu, A. J. M. Plompen, and H. Weigmann, J. Nucl. Sci. Tech. Suppl. **2**, 746 (2002).
[62] M. Avrigeanu, V. Avrigeanu, M. Diakaki, and R. Vlastou, Phys. Rev. C **85**, 044618 (2012).
[63] A. J. Koning, S. Hilaire, and S. Goriely, Nucl. Phys. A **810**, 13 (2008).
[64] T. von Egidy and D. Bucurescu, Phys. Rev. C **80**, 054310 (2009).
[65] M. A. Gardner and D. G. Gardner, Lawrence Livermore National Laboratory Report UCRL-92492, 1985.
[66] D. J. Dean, S. E. Koonin, K. Langanke, P. B. Radha, and Y. Alhassid, Phys. Rev. Lett. **74**, 2909 (1995); K. Langanke, D. J. Dean, S. E. Koonin, and P. B. Radha, Nucl. Phys. A **613**, 253 (1997); Y. Alhassid, G. F. Bertsch, L. Fang, and S. Liu, Phys. Rev. C **72**, 064326 (2005); Y. Alhassid, S. Liu, and H. Nakada, Phys. Rev. Lett. **99**, 162504 (2007).
[67] T. Kawano, P. Talou, and M. B. Chadwick, Nucl. Instrum. Methods A **562**, 774 (2006); D. Dashdorj, T. Kawano, P. E. Garrett, J. A. Becker, U. Agvaanluvsan, L. A. Bernstein, M. B. Chadwick, M. Devlin, N. Fotiades, G. E. Mitchell, R. O. Nelson, and W. Younes, Phys. Rev. C **75**, 054612 (2007); N. Fotiades, R. O. Nelson, M. Devlin, S. Holloway, T. Kawano, P. Talou, M. B. Chadwick, J. A. Becker, and P. E. Garrett, *ibid.* **80**, 044612 (2009).
[68] M. Avrigeanu and V. Avrigeanu, Comp. Phys. Comm. **112**, 191 (1998); A. Harangozo, I. Stetcu, M. Avrigeanu, and V. Avrigeanu, Phys. Rev. C **58**, 295 (1998).
[69] H. Feshbach, A. Kerman, and S. Koonin, Ann. Phys. (NY) **125**, 429 (1980).
[70] C. Y. Fu, Nucl. Sci. Eng. **92**, 440 (1986).
[71] E. Gadioli and E. Gadioli-Erba, Z. Phys. A **299**, 1 (1981).
[72] A. Bohr and B. R. Mottelson, in *Nuclear Structure* (W. A. Benjamin, Inc., New York, 1969), p. 141.
[73] M. Guttormsen *et al.*, Phys. Rev. C **71**, 044307 (2005).
[74] M. Wiedeking *et al.*, Phys. Rev. Lett. **108**, 162503 (2012).
[75] J. Kopecky and M. Uhl, Phys. Rev. C **41**, 1941 (1990).
[76] D. G. Gardner and F. S. Dietrich, LLNL-Livermore Report UCRL-82998, 1979.
[77] M. Avrigeanu, V. Avrigeanu, G. Cata, and M. Ivascu, Rev. Roum. Phys. **32**, 837 (1987).
[78] A. C. Larsen and S. Goriely, Phys. Rev. C **82**, 014318 (2010).
[79] I. Daoutidis and S. Goriely, Phys. Rev. C **86**, 034328 (2012).
[80] M. Beard, S. Frauendorf, B. Kämpfer, R. Schwengner, and M. Wiescher, Phys. Rev. C **85**, 065808 (2012).
[81] M. G. Mustafa, T. Tamura, and T. Udagawa, Phys. Rev. C **35**, 2077 (1987).
[82] H. I. West Jr., R. G. Lanier, and M. G. Mustafa, Phys. Rev. C **35**, 2067 (1987).